(3) Mandelkern, L. *Discuss. Faraday Soc.* **1979**, *No. 68*. See discussion remarks on pp 414-5.
(4) Wunderlich, B. *Discuss. Faraday Soc.* **1979**, *No. 68*. See discussion remarks on pp 417-9.
(5) The T_m' vs. $1/l$ plot[1] gives an estimate of both $T_m°$ and σ_e. The interplay between the $\sigma\sigma_e$ from the kinetic data using this $T_m°$, and the σ_e from the same T_m' vs. $1/l$ plot, is such that σ always falls between about 11 and 14 erg cm^{-2} for $T_m°$ values running from 141.5 to 146.5 °C because of compensating effects in the analysis. All the disputed values of $T_m°$ for polyethylene are within these limits.[3,4]
(6) Point, J. J.; Kovacs, A. J. *Macromolecules* **1980**, *13*, 399.
(7) Leung, W. M.; Manley, R. St. John Post Grad. Lab. Report no. 275; Pulp and Paper Research Institute of Canada, Pointe Claire, Quebec 1983. Three papers based on this work appear immediately preceding this paper in this issue of *Macromolecules*.
(8) Flory, P. J.; Vrij, A. *J. Am. Chem. Soc.* **1963**, *85*, 3548.
(9) Flynn, J. H. *Polymer* **1982**, *23*, 1325.
(10) Lauritzen, J. I., Jr.; Hoffman, J. D. *J. Appl. Phys.* **1972**, *44*, 4340.
(11) In the more general case, the rate constants given in eq 6-9 can be written[1] $A_0 = \beta_g \exp[-2b_0\sigma l_x/kT - 2a_0b_0\sigma'/kT + \psi a_0b_0l_x(\Delta f)/kT]$, $B_1 = \beta_g \exp[-(1-\psi)a_0b_0l_x(\Delta f)/kT]$, $A = \beta_g \exp[-2a_0b_0\sigma'/kT + \psi a_0b_0l_x(\Delta f)/kT]$, and $B = \beta_g \exp[-(1-\psi)a_0b_0l_x(\Delta f)/kT]$ where $0 \le \psi \le 1$. These expressions are consistent with eq 5 and detailed balance for any fixed value of ψ. In the more general case, a different ψ can be assigned to A_0 and B_1 on the one hand, and A and B on the other.[10]
(12) Lauritzen, J. I., Jr.; Passaglia, E.; DiMarzio, E. A. *J. Res. Natl. Bur. Stand., Sect. A* **1967**, *71*, 245.
(13) Lauritzen, J. I., Jr.; DiMarzio, E. A.; Passaglia, E. *J. Chem. Phys.* **1966**, *45*, 4444.
(14) Lauritzen, J. I., Jr. *J. Appl. Phys.* **1973**, *44*, 4353.
(15) Frank, F. C. *J. Cryst. Growth* **1974**, *22*, 233.
(16) Aquilano, D. *J. Cryst. Growth* **1977**, *37*, 215.
(17) Ross, G. S.; Ross, L. F., private communication.
(18) (a) Khoury, F. *J. Appl. Phys.* **1963**, *34*, 73. (b) It is clear from the work of Leung and Manley[7] that prolonged annealing of extended-chain C-207 can lead to the coalescence of the individual platelets producing a (probably somewhat defective) "multilayered" molecular crystal with largely localized chain ends that exhibits an observed dissolution temperature that is far above T_0 and substantially equivalent to $T_d°$. Such crystals must have considerable interpenetration of chain ends from a given interior lamella to the contiguous ones. (See remarks in section II, model B.)
(19) The $c^{0.4}$ concentration dependence of K (and hence the growth rate at a specified $T_0 - T$) may arise from the presence of adsorbed molecules of high surface mobility on the growth surface. This would provide a source of molecules such that the local concentration at the niche is considerably in excess of that in the solution proper, thus giving a K that varied less than the first power of the actual concentration in solution.
(20) Simon, B.; Grassi, A.; Boistelle, R. *J. Cryst. Growth* **1974**, *26*, 77.
(21) Turnbull, D.; Spaepen, F. *J. Polym. Sci., Polym. Symp.* **1978**, *63*, 237.
(22) Oliver, M. J.; Calvert, P. D. *J. Cryst. Growth* **1975**, *30*, 343.
(23) Huseby, T. W.; Bair, H. E. *J. Appl. Phys.* **1968**, *39*, 795.
(24) Keith, H. D.; Passaglia, E. *J. Res. Natl. Bur. Stand., Sect. A* **1964**, *68*, 513.
(25) Hoffman, J. D. *Polymer* **1983**, *24*, 3.
(26) Guttman, C. M.; DiMarzio, E. A.; Hoffman, J. D. *Polymer* **1981**, *22*, 1466.
(27) Mansfield, M. L. *Macromolecules* **1983**, *16*, 914.
(28) Frank, F. C. *Discuss. Faraday Soc.* **1979**, *No. 68*, 7.
(29) Hoffman, J. D. In "Polyethylene 1933-1983", Golden Jubilee Conference, Proceedings of Plastic and Rubber Institute, London, June 1983, pp D3.1 to D3.13.

Rheooptical Response of Rodlike Chains Subject to Transient Shear Flow. 1. Model Calculations on the Effects of Polydispersity

Andrea W. Chow and Gerald G. Fuller*

Department of Chemical Engineering, Stanford University, Stanford, California 94305.
Received July 30, 1984

ABSTRACT: This paper is the first part of a two-part series investigating the flow dynamics of semidilute solutions of rodlike chains. Specifically, the effects of polydispersity are considered. In this paper, numerical solutions of the flow birefringence Δn and the average orientation angle χ for the Doi-Edwards model for monodisperse systems and the Doi-Edwards-Marrucci-Grizzuti model for polydisperse systems are studied. These models, to be tested in part 2 by experimental results on rodlike collagen proteins using the method of two-color flow birefringence, indicate that the rheooptical properties are very sensitive to the high molecular weight components. A polydisperse solution with a small quantity of high molecular weight chains exhibits substantially different behavior than a monodisperse solution, especially under transient flow conditions. In addition, the birefringence overshoot predicted for the rodlike system was found to be much smaller compared to that observed for flexible systems.

Introduction

The flow response to rodlike macromolecules has attracted increased interest recently due to the unique and important properties which can be achieved from incorporating such materials into the processing of a wide range of products. Of particular note is the possibility of producing high-strength fibers and composite materials. Additionally, many biopolymers assume rodlike conformations and the corresponding rheology of these systems is also of interest. In a series of articles, Doi and Edwards[1] have described a molecular model which attempts to describe the dynamics of semidilute solutions of rodlike chains. This model, which is based on the simple rigid-dumbbell model,[2] incorporates a mechanism by which the hindered rotational diffusion of rods in close proximity is accounted for by encapsulating the rods within tubes which restrict their translation normal to the chain axis but leave translation along the axis unaffected. This simple model has been shown to qualitatively predict a variety of observed phenomena including the strong concentration and molecular weight dependencies of many rheological and dynamic properties.[3,4]

In its original form, the Doi-Edwards model of concentrated rodlike chains describes systems of uniform chain length. For dilute solutions in which interparticle interactions are negligible, polydispersity can be treated as a simple extension of the monodisperse case. Any bulk solution property is simply the weighted average of the

0024-9297/85/2218-0786$01.50/0

contributions by the constituent components. Beyond the dilute concentration range, however, polydispersity is a much more complicated problem. Recently, Marrucci and Grizzuti[5,6] have proposed a method to incorporate polydispersity into the Doi–Edwards model. They pointed out that while polydispersity only broadens some features, it can have a dramatic effect on other properties. Using a preaveraging approximation to solve the moment equations that describe the flow behavior of the system, Marrucci and Grizzuti obtained the steady-state solutions for the shear and normal stresses for bi- and trimodal systems to illustrate their points.

This paper is the first in a two-part series describing the response of semidilute rodlike chains subject to transient shear flow. In part 2 the results of experiments utilizing the method of two-color flow birefringence on rodlike collagen proteins will be presented and compared against the Doi–Edwards–Marrucci–Grizzuti (DEMG) model. The technique of flow birefringence provides a number of advantages over the mechanical devices which are used for stress measurements. The temporal response of the mechanical measuring devices is often limited by the inherent compliance of the instrument components which sometimes even distorts the measured signals. The flow birefringence measurements, on the other hand, are localized, nonintrusive, and capable of much faster response times. Consequently, this optical technique provides more precise measurements especially for small signals and for fast, transient flow cases. In this paper the molecular model itself is examined. In particular, the consequence of introducing polydispersity into the model is considered and found to produce qualitative differences in the model predictions for the flow birefringence experiment under transient flow conditions. In addition, the preaveraging technique used by Marrucci and Grizzuti, which saves substantial computation time, has been evaluated against the exact solution. The accuracy and usefulness of this approximation scheme will also be discussed.

Summary of Theories

Doi–Edwards Model for Monodisperse Systems. In the Doi–Edwards model for monodisperse, semidilute rigid-rod polymer solutions, the concentration range considered as

$$1/L^3 \ll c \ll 1/dL^2 \tag{1}$$

where c is the concentration in number of rods per unit volume, L is the length, and d is the diameter of the thin rods ($d \ll L$). The lower concentration limit means that the rods are interacting with their neighbors, and the upper limit restricts the concentration to that below the isotropic–nematic phase transition so that the solution can still be considered thermodynamically ideal at equilibrium.

In this model the steric hindrance imposed by neighboring rods is incorporated by enclosing a test rod within an imaginary tube, the dimensions of which are specified by the concentration and length of the rods. The encapsulated rod is allowed to diffuse freely along its axis, but diffusion perpendicular to the axis is restricted. In order for the test rod to perform an elementary rotation, either the test rod or the impeding rod has to diffuse a distance of order L to free the constraint. As a result, the rotary diffusion coefficient for the rods is lowered. If the test rod is assigned an orientation vector $\mathbf{u}(t)$, the diffusion equation governing the orientation probability distribution function, $f(\mathbf{u},t)$, of the rod is given by

$$\frac{\partial f(\mathbf{u},t)}{\partial t} + \text{div}\,(f\dot{\mathbf{u}}(t) - \tilde{D}_r \nabla f) = 0 \tag{2}$$

$$\dot{\mathbf{u}}(t) = \mathbf{g}(t)\cdot\mathbf{u}(t) - (\mathbf{u}\cdot\mathbf{g}\cdot\mathbf{u})\mathbf{u} \tag{3}$$

where $\mathbf{g}(t)$ is the velocity gradient tensor of the applied flow field and $\tilde{D}_r$ is the rotary diffusion coefficient of the rods. The second term in the diffusion equation (eq 2) accounts for the convective flux due to the flow while the third term represents the diffusive flux due to Brownian motions. This diffusion equation has a form identical with that for an isolated, rigid dumbbell,[2] except that the diffusion coefficient $\tilde{D}_r$ is given by

$$\tilde{D}_r(\mathbf{u},[f]) = D_r\left[(4/\pi)\int d^2\mathbf{u}'\, f(\mathbf{u}',t)\,\sin\,(\mathbf{u}\mathbf{u}')\right]^{-2} \tag{4}$$

Here, the symbol $(\mathbf{u}\mathbf{u}')$ denotes the angle between the test rod and a neighboring rod with orientation vector $\mathbf{u}'$. D_r is the rotary diffusion coefficient for a quiescent concentrated solution, which is related to D_{r0}, the diffusion coefficient for a single, isolated rod, by the following relation:

$$D_r = \beta(cL^3)^{-2}D_{r0} \tag{5}$$

Here β is an undetermined numerical constant. Thus, eq 4 accounts for the hindered rotation of the test rod resulting from the close proximity of neighboring rods.

If one can solve the time-dependent kinetic equations, eq 2–4, with the appropriate initial conditions, moments of the probability function f can be obtained. Consequently, many of the bulk solution properties, such as the flow birefringence and the orientation angle, can be predicted.

DEMG Model for Polydisperse Systems. In a polydisperse solution where rods of different lengths coexist, a test rod of length L_i can be hindered by rods of any length L_j. To remove this constraint, either the impeding rod or the test rod itself must diffuse longitudinally a distance of order of its own length. These two processes are no longer equivalent as in the monodisperse case. The faster of the two diffusion processes determines the characteristic time needed for the test rod to perform an elementary rotation. Equation 4 describing the rotational diffusivity is then replaced by the following expression for the i-rod of length L_i:[5,6]

$$D_{ri} \sim \tilde{L_i^{-4}}\left(\sum_m c_m L_m \langle \sin\,(\mathbf{u}\mathbf{u}')\rangle_m\right)^{-1}\left\{\sum_{j\le i} c_j L_j^3 \langle \sin\,(\mathbf{u}\mathbf{u}')\rangle_j / D_{tj} + (L_i^2/D_{ti})\sum_{j>i} c_j L_j \langle \sin\,(\mathbf{u}\mathbf{u}')\rangle_j\right\}^{-1} \tag{6}$$

Here, c_m is the number concentration of the m-rods, and D_{tm} is the translational diffusivity of an isolated m-rod. In addition, it is understood that $j \le i$ implies $L_j \le L_i$. The angular brackets $\langle\rangle_m$ refer to the configurational average over $f_m(\mathbf{u},t)$ which is the probability that a rod of length L_m has an orientation $\mathbf{u}$ at time t.

Methods of Solution

Infinite Series Expansion. Doi and Edwards have solved the monodisperse problem by the method of infinite series expansion for simple shear flow.[1,7] The details of the mathematics can be found in their papers and we will only summarize their results here.

A simplifying approximation is first made to replace the orientation-dependent diffusion constant $\tilde{D}_r(\mathbf{u},[f])$ by an effective diffusion constant $\bar{D}_r$ that only depends on the shear rate g:

$$\bar{D}_r = \langle \tilde{D}_r \rangle = D_r\left[(4/\pi)\int d^2\mathbf{u}\, d^2\mathbf{u}'\, f(\mathbf{u})\, f(\mathbf{u}')\,\sin\,(\mathbf{u}\mathbf{u}')\right]^{-2} \tag{7}$$

The orientation probability $f(\mathbf{u},t)$ is then expanded in terms of an infinite series of spherical harmonics $Y_{lm}(\Theta,\Phi)$

$$f(t;\Theta,\Phi) = \sum_{l=0}^{\infty}\sum_{m=0}^{l} b_{lm}(t)|lm\rangle \tag{8}$$

where

$$|lm\rangle = Y_{lm}(\Theta,\Phi) \qquad \text{for } m = 0$$

$$= (1/2^{1/2})[Y_{lm}(\Theta,\Phi) + (-1)^m Y_{l-m}(\Theta,\Phi)] \qquad \text{for } 1 \le m \le l$$

Such an expansion reduces the partial differential equation of eq 2 into a set of nonlinear, ordinary, first-order differential equations for the time-dependent coefficients b_{lm}

$$db_{lm}(t)/dt = -\bar{D}_r l(l+1)b_{lm} - g\sum_{l'=0}^{\infty}\sum_{m'=0}^{l}(lm|\Gamma|l'm')b_{l'm'} \tag{9}$$

where

$$\bar{D}_r = D_r\left(1 - 8\pi\sum_{l=2}^{\infty}\sum_{m=0}^{l}\left(\frac{l-1}{l+2}\right)\left[\frac{(l-3)!!}{l!!}\right]^2|b_{lm}|^2\right)^{-2} \tag{10}$$

The operator Γ and the matrix element $(lm|\Gamma|l'm')$ are defined in eq B.1–B.4 of ref 1.

With the appropriate initial conditions $b_{lm}(0)$, eq 9 and 10 can be solved by truncating b_{lm} at $l = l_{max}$. In our calculations, l_{max} was taken as 12–24 depending on the shear rate. From the normalization condition of the probability function, $b_{00} = 1/(4\pi)^{1/2}$. All other coefficients b_{lm} are zero at the isotropic state.

Using the Lorentz–Lorenz rule which assumes coaxiality of the molecular polarizability tensor and the refractive index tensor, one can relate the birefringence Δn and the orientation angle χ to the moments of f as follows:

$$\Delta n = cM[\langle u_x^2 - u_y^2\rangle^2 + 4\langle u_x u_y\rangle^2]^{1/2} \tag{11}$$

$$\chi = \tfrac{1}{2}\tan^{-1}(\langle u_x u_y\rangle/\langle u_x^2 - u_y^2\rangle) \tag{12}$$

where M is a constant associated with the intrinsic anisotropy of the polarizability of the polymer solution. u_x and u_y are the components of the unit vector of the test rod along the flow and shear directions, respectively. They are related to the coefficients b_{lm} by

$$\langle u_x u_y\rangle = -(4\pi/15)^{1/2}b_{21} \tag{13}$$

$$\langle u_x^2 - u_y^2\rangle = (4\pi/15)^{1/2}(b_{22} - 3^{1/2}b_{20}) \tag{14}$$

The above problem has been nondimensionalized by the characteristic time D_r^{-1} and the characteristic length L.

We have followed a similar procedure to solve the diffusion equations for the DEMG model. The characteristic time and length scales for the polydisperse system, following Marrucci and Grizzuti's notation, are now defined as

$$\bar{D}_r^{-1} = (\sum_m c_m/D_{0m}^2)/(\sum_m c_m/D_{0m}) \tag{15}$$

$$\bar{L}^2 = (1/c)\sum_m c_m L_m^2 \tag{16}$$

where D_{0i} is the rotational diffusivity at isotropic conditions defined as

$$D_{0i} = \beta\frac{kT}{\eta_s}\frac{1}{c\bar{L}}L_i^{-4}\{\sum_{j\le i} c_j L_j^4 + L_i^3\sum_{j>i} c_j L_j\}^{-1} \tag{17}$$

Here, k is the Boltzmann constant, T is the absolute temperature, η_s is the solvent viscosity, β is a proportionality constant, and

$$c = \sum_m c_m, \qquad \bar{L} = (1/c)\sum_m c_m L_m \tag{18}$$

For the polydisperse system, each probability function f_i for rods of length L_i is expanded in spherical harmonics. This procedure yields a system of equations for each set of coefficients $b_{lm,i}$

$$b_{lm,i}(t)/dt = -\bar{D}_{ri}l(l+1)b_{lm,i} - g\sum_{l'=0}\sum_{m'=0}(lm|\Gamma|l'm')b_{lm,i} \tag{19}$$

$$\bar{D}_{ri} \sim L_i^{-4}(\sum_m c_m L_m Q_{im})^{-1}\{\sum_{j\le i} c_j L_j^3 Q_{ij} + L_i^4\sum_{j>i} c_j L_j Q_{ij}\}^{-1} \tag{20}$$

$$Q_{ij} = 1 - 8\pi\sum_{l=2}^{\infty}\sum_{m=0}^{l}\left(\frac{l+1}{l+2}\right)\left(\frac{(l+3)!!}{l!!}\right)^2 b_{lm,i}b_{lm,j} \tag{21}$$

Although the above procedure does contain the simplifying assumption of eq 7, it shall be referred to in later sections as the "exact" solution in comparison to the preaveraging approximation described in the next section. The equations relating Δn and χ to $b_{lm,i}$ become

$$\Delta n = cM\{[\sum_m c_m L_m\langle u_x^2 - u_y^2\rangle_m]^2 + 4[\sum_m c_m L_m\langle u_x u_y\rangle_m]^2\}^{1/2} \tag{22}$$

$$\chi = \tfrac{1}{2}\tan^{-1}(2\sum_m c_m L_m\langle u_x u_y\rangle_m/\sum_m c_m L_m\langle u_x^2 - u_y^2\rangle_m) \tag{23}$$

$$\langle u_x u_y\rangle_i = -(4\pi/15)^{1/2}b_{21,i} \tag{24}$$

$$\langle u_x^2 - u_y^2\rangle_i = (4\pi/15)^{1/2}(b_{22,i} - 3^{1/2}b_{20,i}) \tag{25}$$

Preaveraging Approximation. In order to facilitate the solution of the equations governing the time evolution of the moments of the orientation distribution function, Doi[8] has introduced a preaveraging approximation which has been worked out in detail for both the monodisperse and polydisperse cases by Marrucci and Grizutti.[6] An order parameter tensor $\boldsymbol{S}$ is introduced:

$$\boldsymbol{S} = \langle \mathbf{uu} - \tfrac{1}{3}\boldsymbol{I}\rangle \tag{26}$$

When eq 2 is multiplied throughout by $\mathbf{uu} - {}^1/_3\boldsymbol{I}$ and integrated over $\mathbf{u}$, the resulting equation contains a fourth-order tensor $\langle \mathbf{uuuu}\rangle$. This tensor is then approximated by the second-order tensor $\langle \mathbf{uu}\rangle$ as follows:

$$\langle \mathbf{uuuu}\rangle = \langle \mathbf{uu}\rangle\langle \mathbf{uu}\rangle \tag{27}$$

As a result, the diffusion equation for the monodisperse solutions becomes

$$d\boldsymbol{S}/dt = -6\bar{D}_r\boldsymbol{S} + \boldsymbol{G}(\boldsymbol{S}) \tag{28}$$

where

$$\boldsymbol{G}(\boldsymbol{S}) = \tfrac{1}{3}(\boldsymbol{g} + \boldsymbol{g}^+) + \boldsymbol{g}\cdot\boldsymbol{S} + \boldsymbol{S}\cdot\boldsymbol{g}^+ - \tfrac{2}{3}(\boldsymbol{g}:\boldsymbol{S})\boldsymbol{I} - 2(\boldsymbol{g}:\boldsymbol{S})\boldsymbol{S} \tag{29}$$

with $\boldsymbol{g}^+$ and transpose of $\boldsymbol{g}$. The rotational diffusivity may now be written as

$$\bar{D}_r = D_r(1 - \tfrac{3}{2}\boldsymbol{S}:\boldsymbol{S})^{-2} \tag{30}$$

As explained in ref 6, the constant ${}^3/_2$ corresponds to the limit of strong alignment of all rods. At the weak-flow limit where the system is near isotropic state, the constant should be replaced by 15/16.

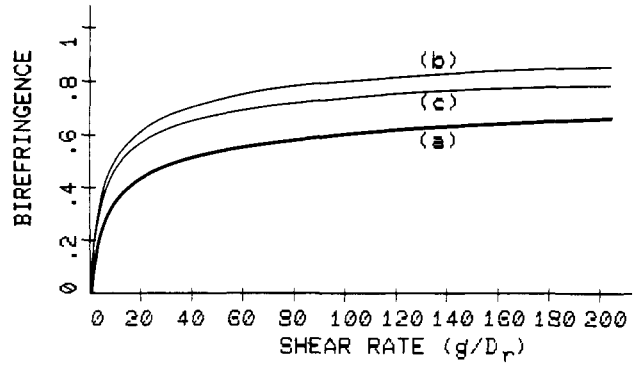

Figure 1. Steady-state birefringence as a function of the dimensionless shear rate by the Doi–Edwards model: (a) Exact solution, (b) weak-flow preaveraged approximation, and (c) strong-flow preaveraged approximation.

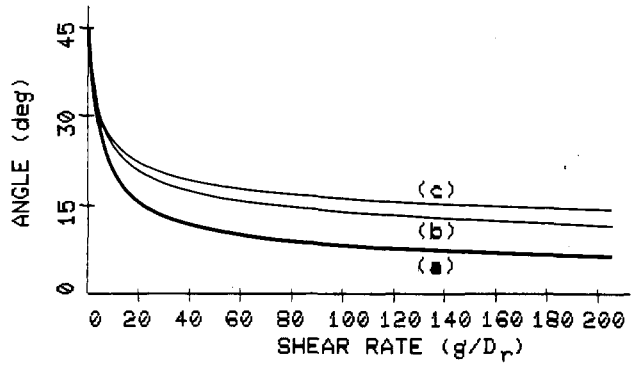

Figure 2. Steady-state angle of orientation as a function of the dimensionless shear rate by the Doi–Edwards model. The notations are the same as in Figure 1.

When the above manipulation is extended to the DEMG model, the equation describing the rate of change of $\boldsymbol{S}_i$ for the i-rods is

$$d\boldsymbol{S}_i/dt = -6\bar{D}_r\boldsymbol{S}_i + \boldsymbol{G}(\boldsymbol{S}_i) \quad (31)$$

where $\boldsymbol{S}(\boldsymbol{S}_i)$ is the same function as eq 29. The average rotational diffusivity for the i-rods is

$$\bar{D}_{ri} \sim L_i^{-4}\left\{\sum_m c_m L_m\left(1 - \frac{15}{16}\boldsymbol{S}_i:\boldsymbol{S}_m\right)\right\}^{-1}\left\{\sum_{j\le i} c_j L_j^4\left(1 - \frac{15}{16}\boldsymbol{S}_i:\boldsymbol{S}_j\right) + L_i^3\sum_{j>i} c_j L_j\left(1 - \frac{15}{16}\boldsymbol{S}_i:\boldsymbol{S}_j\right)\right\}^{-1} \quad (32)$$

In the isotropic state, the order parameter tensor is zero. The birefringence and the orientation angle can be calculated from eq 22 and 23.

Numerical Solutions

Monodisperse Solution. Figures 1 and 2 are the Doi–Edwards model predictions of the steady-state birefringence and orientation angle as a function of the normalized shear rate, g/D_r. In these two plots, curve a is the numerical solution using the method of infinite series expansion; curves b and c are the weak- and strong-flow approximations using the preaveraging technique. The model predicts that the birefringence increases monotonically with the shear rate as more and more rods are aligned by the flow. The function levels off at higher shear rate when the orientation effect saturates. The average orientation angle, on the other hand, decreases sharply at low shear rate and then approaches zero asymptotically at infinite value of g/D_r, at which all the rods are aligned in the flow direction.

The preaveraging approximation, using either the weak-flow or the strong-flow limit, overestimates the birefringence over the whole range of g/D_r. The discrepancy is as high as 70%. The orientation angle predicted by the approximation is also always higher than the exact solution.

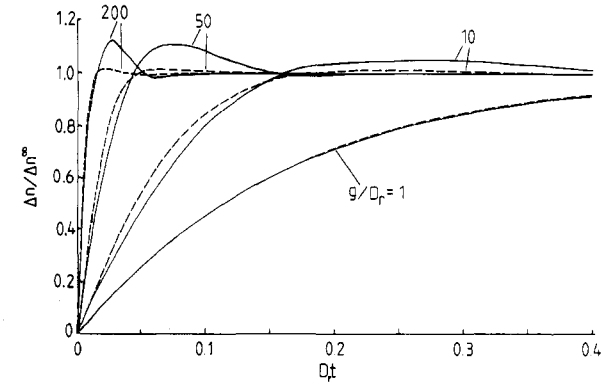

Figure 3. Birefringence as a function of the dimensionless time upon the inception of shear flow by the Doi–Edwards model. Solid line is the exact solution and the broken line is the weak-flow preaveraged approximation.

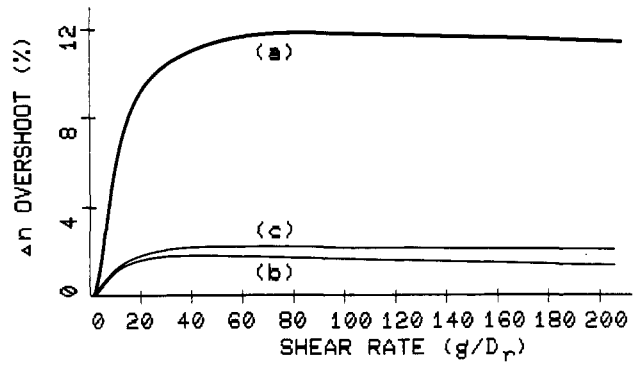

Figure 4. Percent overshoot in the birefringence upon the inception of shear as a function of the dimensionless shear rate predicted by the Doi–Edwards model. The notations are the same as in Figure 1.

Figure 3 is a plot of the time-dependent birefringence following the inception of shear at different values of g/D_r. The birefringence has been normalized by the steady-state value at that shear rate, and time has been normalized by the characteristic time scale D_r^{-1}. The solid lines in this figure are the exact solutions, and the broken lines are the weak-flow preaveraged approximations. The strong-flow preaveraged approximation consistently gives poorer agreement with the exact solution because simple shear flow is inherently a weak flow. At $g/D_r \le 1$ where the convective time scale is greater than or comparable to the diffusive time scale, the birefringence is a monotonically increasing function with time. At higher values of g/D_r, however, Δn exhibits an overshoot before it levels off to its steady-state value. This overshoot occurs because the convective time scale is now less than the diffusive time, and therefore the orientation effect by the flow dominates at short time. The magnitude of the overshoot is calculated to be as high as ~12% by the eact solution. This overshoot is very small in contrast with that exhibited by flexible systems, which are capable of an additional mode of deformation by stretching from the coiled configuration. For polystyrene, the overshoot in the birefringence has been reported to be as high as 250% following the inception of high shear rates.[9]

The solution based on the preaveraging approximation, on the other hand, deviates quite markedly from the exact solution. The magnitude of the overshoot is always underestimated as summarized in Figure 4. In this figure,

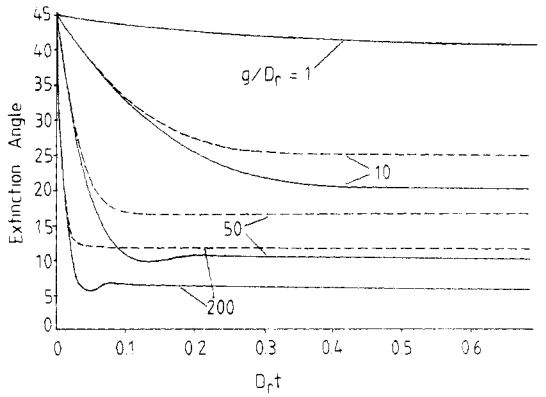

Figure 5. Orientation angle as a function of the dimensionless time by the Doi–Edwards model. The notations are the same as in Figure 3.

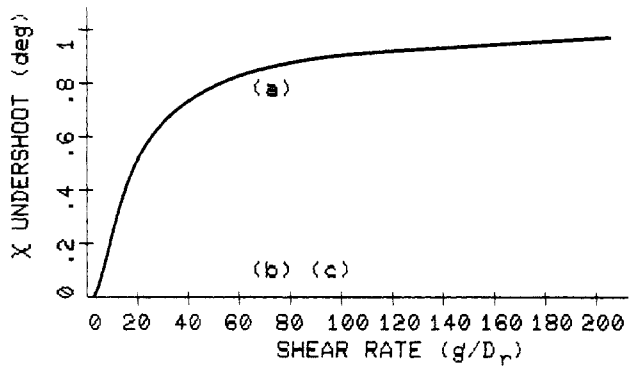

Figure 6. Undershoot in the angle of orientation upon the inception of shear as a function of the dimensionless shear rate predicted by the Doi–Edwards model. The notations are the same as in Figure 1.

curve a is again the exact solution, and curves b and c are the weak- and strong-flow preaveraged approximations. Moreover, the estimated temporal position at which the maximum of the overshoot occurs differs from the eact solution by as much as 20%.

Figure 5 is a plot of the orientation angle vs. time following the inception of shear. The angle also exhibits nonlinear behavior as an undershoot is predicted at high values of g/D_r. The preaveraged-approximation solutions, however, show an undershoot in the angle 2 orders of magnitude smaller than the prediction by the exact solution. It is practically zero in Figure 6 (curves b and c), where the undershoot is plotted as a function of the applied shear rate. The time at which the undershoot occurs is overestimated by the preaveraged approximation by $\sim$ 30% over the range of g/D_r studied.

Following the cessation of shear, the birefringence is predicted to relax back to the isotropic state as in Figure 7. The exact solution (solid line) indicates a shear-rate-insensitive relaxation rate, while the preaveraged-approximation solution (broken line) predicts a stronger dependence of the relaxation rate on the applied shear rate. The orientation angle, on the other hand, is predicted by both solutions to remain unchanged from its value prior to the cessation of flow during the relaxation process. The angle remains unchanged because there is an equal likelihood that the rods will disorient by rotating in any direction.

From the above comparison of the preaveraging approximations to the exact solution, we conclude that both the strong-flow and the weak-flow approximations resemble the exact solution qualitatively for both steady-state and transient flow conditions. Quantitatively, however,

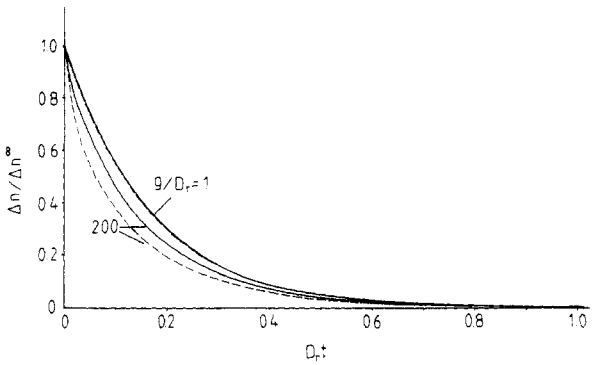

Figure 7. Birefringence as a function of time upon the cessation of flow by the Doi–Edwards model. The notations are the same as in Figure 3.

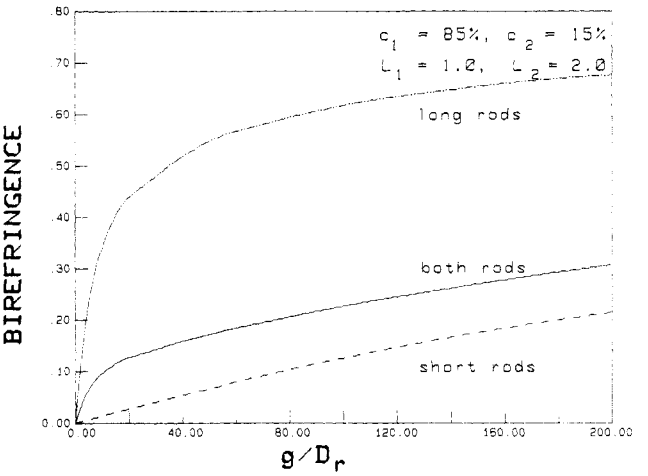

Figure 8. Steady-state birefringence for a bimodal system of 85% short rods and 15% long rods predicted by the DEMG model.

the comparison is poor. The preaveraging approximation, while preserving the overshoot and undershoot in the birefringence and orientation angle, substantially reduces these features. Similar results were reported by Leal and Hinch[10] in their attempt to solve the diffusion equation for dilute suspensions of rigid spheroidal particles (which reduces to the rigid-dumbbell model when the particle aspect ratio approaches infinity). They have tried various forms using the second-order tensor $\langle \mathbf{uu} \rangle$ to approximate the fourth-order tensor $\langle \mathbf{uuuu} \rangle$ but found only fair quantitative agreement between the preaveraged approximations and the exact solution. The peraveraging-approximation scheme is nonetheless useful for a quick qualitative estimate of the model predictions since the requuired computing time is 3–4 orders of magnitude shorter than that needed for the exact solution.

Polydisperse Solutions. The Doi–Edwards theory suggests a strong length dependence of the rotational diffusivity. As a result, in a bimodal system where two different rod lengths coexist, the dynamics of the two constituents can be drastically different from one another. This disparity brings forth some interesting results that are not predicted by the monodisperse model.

In the last section, the preaveraging technique of eq 27 has been found to be only a fair approximation of the exact solution. Consequently, the solutions discussed in this section are based on the method of infinite series expansion. Figures 8 and 9 are plots of the steady-state birefringence and orientation angle for a bimodal system that consist of 85% rods of length L_1 and 15% rods of length L_2. In this examaple, L_2 is twice L_1. This particular bimodal distribution was chosen as it corresponds to one of

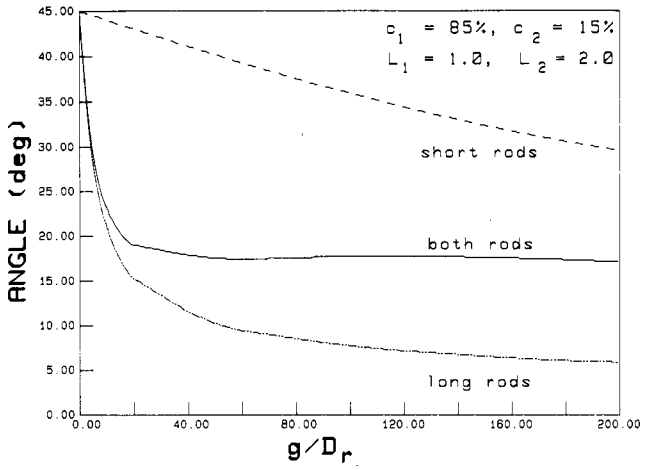

Figure 9. Steady-state angle of orientation for a bimodal system of 85% short rods and 15% long rods by the DEMG model.

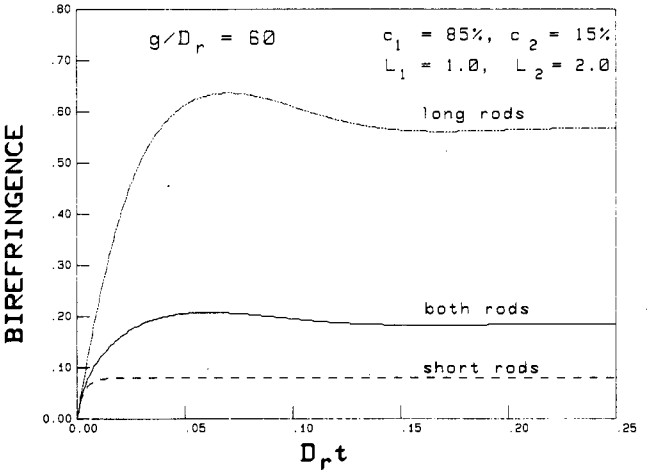

Figure 10. Time-dependent birefringence upon the inception of shear with $g/D_r = 60$ for a bimodal system of 85% short rods and 15% long rods by the DEMG model.

the experimental systems discussed in part 2. In this case, the rotational diffusivity of the short rods, D_{r1}, is 30–50 times higher than that of the long rods, D_{r2}. The solid lines in these two plots show the change in Δn for the bimodal system as a function of g/D_r, where D_r is the average rotational diffusivity as defined in eq 15–18. Since D_{ri} is much lower, the effective shear rate experienced by the long rods (g/D_{r2}) is much higher than the effective shear rate experienced by the short rods (g/D_{r1}). Consequently, the long rods are always more aligned and are oriented at a lower angle than the shorter rods at any given value of g/D_r.

For this sample bimodal system, Figure 8 shows that the birefringence is a monotonically increasing function of the shear rate. However, the shape of the function is different from that characterizing the monodisperse system. At high shear rate, the average Δn does not level off but rather increases at a moderate rate over a wide range of g/D_r until the orientation effect of the short rods also saturates.

The orientation angle, as shown in Figure 9, exhibits more peculiar behavior. The average angle (solid line) first drops rapidly at low shear rate where the dynamics of the long rods dominate. The function then shows a slight increase before it decreases again at very high shear rates. This is because at lower values of g/D_r the measured angle is more greatly influenced by the longer rods which are more highly aligned and at a lower angle than the shorter rods. As the shear rate increases, more short rods are oriented, and therefore the statistical average places a

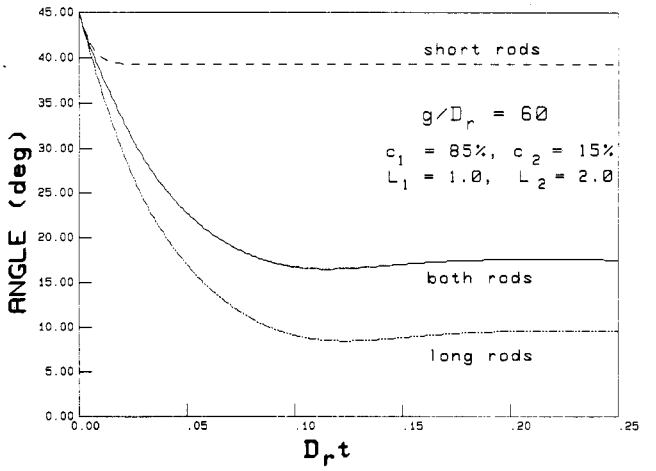

Figure 11. Time-dependent angle of orientation upon the inception of shear with $g/D_r = 60$ for a bimodal system of 85% short rods and 15% long rods by the DEMG model.

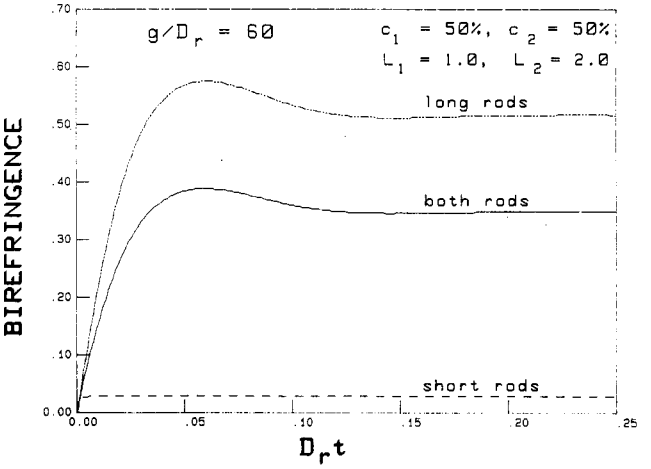

Figure 12. Time-dependent birefringence upon the inception of shedar with $g/D_r = 60$ for a bimodal system of 50% short rods and 50% long rods by the DEMG model.

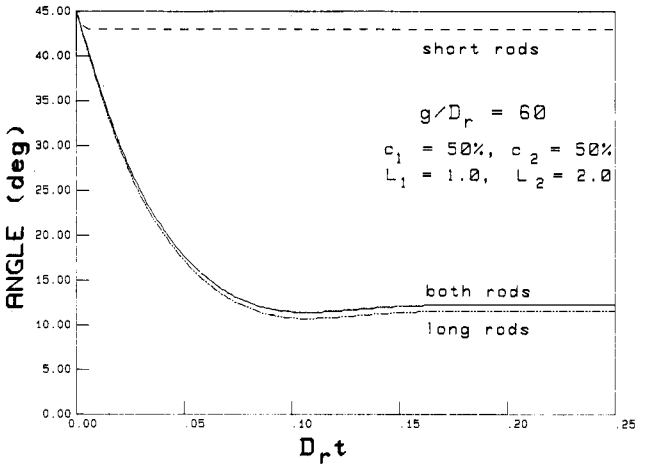

Figure 13. Time-dependent orientation angle upon the inception of shear with $g/D_r = 60$ for a bimodal system of 50% short rods and 50% long rods by the DEMG model.

greater weight on the contribution from the short rods. A local maximum in the orientation angle occurs when the dynamics of the short rods begin to dominate.

Figures 10 and 11 are the time-dependent plots of the birefringence and the orientation angle of the sample bimodal system following the inception of shear with $g/D_r = 60$. These two plots show somewhat unexpected results

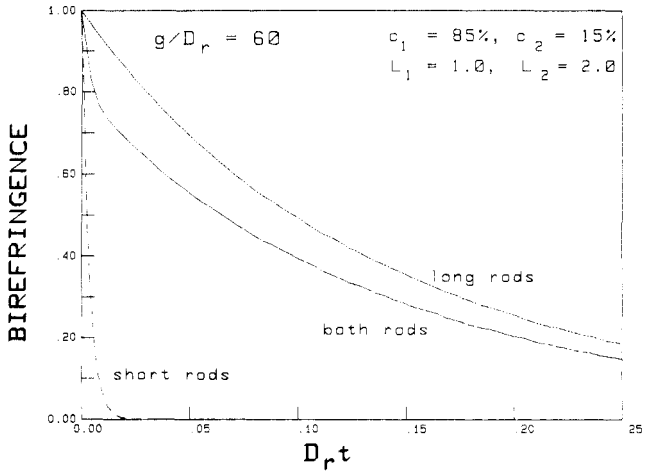

Figure 14. Time-dependent birefringence upon the cessation of shear with $g/D_r = 60$ for a bimodal system of 85% short rods and 15% long rods by the DEMG model. The birefringence has been normalized by its steady-state value prior to the cessation of flow.

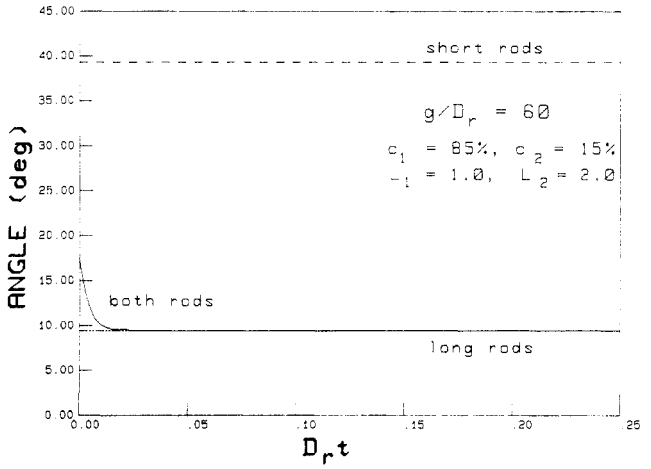

Figure 15. Time-dependent orientation angle upon the cessation of shear with $g/D_r = 60$ for a bimodal system of 85% short rods and 15% long rods by the DEMG model.

in that the time-dependent behavior of the mixture is more sensitive to the dynamics of the long rods, even though they only account for 15% of the total number concentration. Figures 12 and 13 show similar time-dependent functions for another bimodal system consisting of 50% single rods and 50% double rods. In this case the dynamics of the mixture almost entirely resemble those of the long rods.

Since polydispersity introduces multiple relaxation times, the relaxation process of a olydisperse system is dramatically different from that predicted for a monodisperse system. Figure 14 is a plot of the normalized birefringence following the cessation of shear at $g/D_r = 60$. Since the two diffusive time scales, D_{r1}^{-1} and D_{r2}^{-1}, are well separated, the relaxation of Δn is characterized by two distinct relaxation rates. The function Δn (solid line of Figure 14) shows a rapid initial drop followed by a much sloer decay. The orientation angle, shown as Figure 15, exhibits a decrease during the relaxation process when polydispersity is included. The decrease in the angle is also the result of having two relaxation times. Upon the cessation of flow, the short rods are disoriented by the Brownian motions at a much faster rate. As a result, the statistical average of the orientation angle shifts to the orientation of the long rods with time until the short rods are totally relaxed. At this point, the angle remains constant at the average orientation of the long rods.

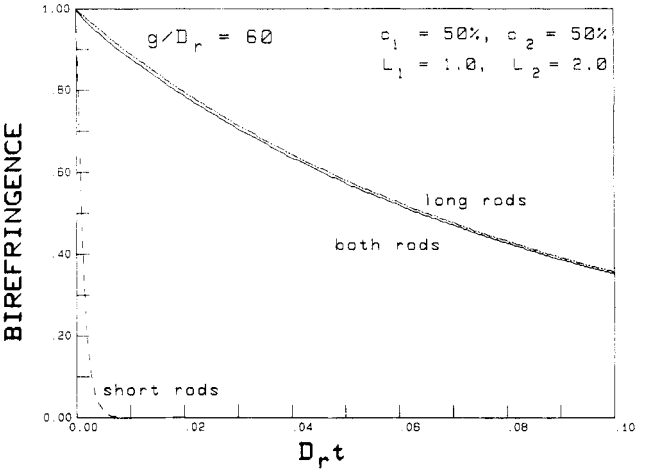

Figure 16. Time-dependent birefringence (normalized by the steady-state value) upon the cessation of shear with $g/D_r = 60$ for a bimodal system of 50% short rods and 50% long rods by the DEMG model.

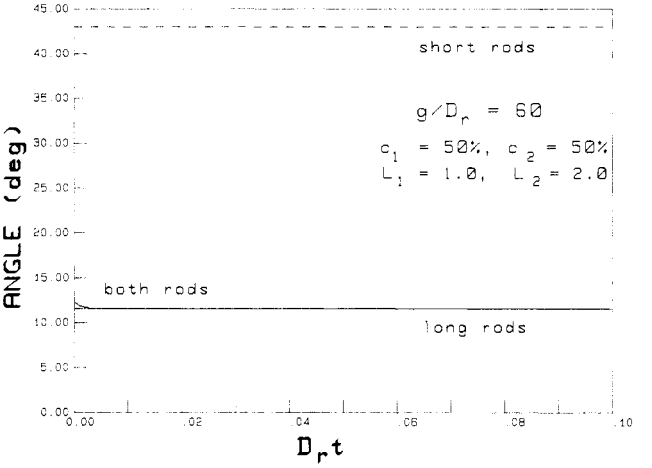

Figure 17. Time-dependent orientation angle upon the cessation of shear with $g/D_r = 60$ for a bimodal system of 50% short rods and 50% long rods by the DEMG model.

Figures 16 and 17 are plots of the relaxation behavior of the bimodal system containing an equal number of single and double rods following the cessation of shear with $g/D_r = 60$. These two figures again indicate that the time-dependent flow properties of a polydisperse system areemuch more sensitive to the contribution from the long rods. The decrease in the angle during relaxation for this particular composition, as shown in Figure 17, is much smaller than that for the other solution shown in Figure 15.

Summary

We have examined the predictions of the flow dynamics of rodlike chains in semidilute solutions by the Doi–Edwards model and the DEdMG model. Specifically, we have calculated the numerical solutions of the flow birefringence and the average orientation angle using two different methods of solution. The dynamics of a polydisperse system were found to be very sensitive to the presence of the high molecular weight chains. The numerical solutions indicated that a polydisperse system with a small amount of longer chains exhibits very different flow properties from its monodisperse counterpart, especially under transient flow conditions. In particular, the orientation angle for a polydisperse system always exhibits decrease during the relaxattion process, while this angle is predicted to remain

unchanged for a monodisperse system. Moreover, a local maximum in the steady-state angle can occur when the statistical average shifts its weight with shear rate from longer rods to shorter rods. Additionally, both the Doi–Edwards and the EEMG models predict a substantially smaller overshoot in the birefringence compared to that measured for flexible systems.

We have also shown that the preaveraging approximation using eq 27 to solve the diffusion equation produces very poor quantitative predictions. It does, however, provide a quick way to estimate the flow properties qualitatively.

In the second part of this series, the DEMG model will be tested against the transient flow results obtained on rodlike collagen proteins using the method of two-color flow birefringence by which fast, transient-flow measurements are possible.

Acknowledgment. This work was supported by the NSF-MRL Program through the Center for Materials Research at Stanford University. Partial support was also obtained from the National Science Foundation (Grant No. NSF-CPE80-25833) and from the ARCO Foundation. In addition, we thank Professor G. Marrucci for his helpful discussion and the preprint of his paper.

References and Notes

(1) Doi, M.; Edwards, S. F. *J. Chem. Soc., Faraday Trans. 2* **1978**, *74*, 560, 918.
(2) Bird, R. B.; Hassager, O.; Armstrong, R. C.; Curtiss, C. F. "Dynamics of Polymer Liquids: Kinetic Theory"; Wiley: New York, 1977.
(3) Chu, S. G.; Venkatraman, S.; Berry, G. C.; Einaga, Y. *Macromolecules* **1981**, *14*, 939.
(4) Zero, K. M.; Pecora, R. *Macromolecules* **1982**, *15*, 87.
(5) Marrucci, G.; Grizzuti, N. *J. Polym. Sci., Polym. Lett. Ed.* **1983**, *21*, 83.
(6) Marrucci, G.; Grizzuti, N. *J. Non-Newtonian Fluid Mech.* **1984**, *14*, 13.
(7) Kuzuu, N. Y.; Doi, M. *Polym. J.* **1980**, *12*, 883.
(8) Doi, M. *Ferroelectrics* **1980**, *30*, 247; *J. Polym. Sci., Polym. Phys. Ed.* **1981**, *19*, 229.
(9) Zebrowski, B. F.; Fuller, G. G., submitted for publication in *J. Polym. Sci., Polym. Phys. Ed.*
(10) Hinch, E. J.; Leal, L. G. *J. Fluid Mech.* **1976**, *76-1*, 187.

Rheooptical Response of Rodlike Chains Subject to Transient Shear Flow. 2. Two-Color Flow Birefringence Measurements on Collagen Protein

Andrea W. Chow and Gerald G. Fuller*

Department of Chemical Engineering, Stanford University, Stanford, California 94305

Donald G. Wallace

Collagen Corporation, Palo Alto, California 94303

Joseph A. Madri

Department of Pathology, Yale University School of Medicine, New Haven, Connecticut 06510. *Received July 30, 1984*

ABSTRACT: Two-color flow birefringence measurements under steady-state and transient shear flow have been obtained on two collagen samples with different molecular weight distributions. The results have been compared to models describing solutions of strongly interacting rodlike polymers, the Doi–Edwards and Doi–Edwards–Marrucci–Grizzuti (DEMG) models, which were studied in detail in part 1 of this two-part series. We have found that only the DEMG model is successful in describing the flow dynamics of the polydisperse collagen solutions. Quantitative comparison of the model to the steady state and the inception of shear results is very good, and the agreement is somewhat poorer with data obtained upon the cessation of shear flow. The quantitative discrepancies in the comparison could be attributed to the finite but limited flexibility of the collagen molecules.

Introduction

The flow response of rodlike and semiflexible polymer chains is of importance to a number of processes utilizing both synthetic and naturally occurring materials to fabricate products with important and unique properties. For example, ultrahigh-strength fibers can be spun from solutions of rodlike aromatic polymer molecules and the possibility of producing such fibers has attracted a great deal of interest from the aircraft and automotive industries.[1] On the other hand, several naturally occurring macromolecules (some proteins and viruses) have rodlike or semiflexible conformations and the flow properties of such systems are also of interest. Collagen protein is one specific example of such a macromolecule which has found application in the fabrication of artificial skin for use in the treatment of burns[2] and as an injectable substance in many cosmetic and reconstructive surgery applications.[3]

The addition of stiff macromolecules in moderate concentration, below any liquid crystalline formation, leads to profound changes in the flow properties of these solutions. Subsequently, there has been a marked increase in the research directed toward understanding the dynamics of rodlike polymer solutions in the semidilute regime. Advances in both experimental and theoretical approaches have been made in recent years, especially with regard to the nature of the interactions between separate chains and

0024-9297/85/2218-0793$01.50/0